Iranian Journal of Medical Physics

ijmp.mums.ac.ir

Development of In-House Head Computed Tomography Dose Index Phantoms Based on Polyester-Resin Materials

Rin Hafsahtul Asiah[1], Heri Sutanto[1], Choirul Anam[1*], Zaenal Arifin[1], Bahrudin[2], Rumaisya Hilmawati[1]

1. Department of Physics, Faculty of Sciences and Mathematics, Diponegoro University, Jl. Prof. Soedarto SH, Tembalang, Semarang 50275, Central Java, Indonesia.
2. Departement of Chemical Engineering, Riau University, Indonesia

ARTICLE INFO

Article type:
Original Paper

Article history:
Received: Nov 14, 2019
Accepted: Mar 16, 2020

Keywords:
X-ray Computed Tomography
Radiation Dosimetry
Radiation Dosage
CTDI Phantom

ABSTRACT

Introduction: Computed tomography dose index (CTDI) phantoms are used to optimize CT examinations in terms of image quality and the received dose. In this study, we aimed to develop cost-effective head CTDI phantoms from polyester-resin (PESR) materials as alternative phantoms.

Material and Methods: The PESR was mixed with methyl ethyl ketone peroxide (MEKP) as a catalyst. The ratios of MEKP to PESR were 1:150, 1:200, 1:250, and 1:300, respectively. The phantom dimensions were designed similar to the standard CTDI phantom, i.e., length of 15 cm and diameter of 16 cm with five holes (diameter, 1.31 cm). The CTDI measurements using the PESR-MEKP phantoms were compared with the CTDI measurements using the standard polymethyl methacrylate (PMMA) phantom.

Results: The results showed that the CTDI values of the PESR-MEKP phantoms were slightly higher (up to 6%) than the standard PMMA phantom. It was found that the CTDI measured by the PESR-MEKP phantom with a ratio of 1:300 had the least significant difference from the standard PMMA phantom; also, at this ratio, the phantom was the most homogeneous.

Conclusion: The head CTDI phantoms based on PESR-MEKP materials were developed and evaluated in this study. It was found that the PR-MEKP phantom with a MEKP-to-PESR ratio of 1:300 was insignificantly different from the standard PMMA phantom. Also, the phantom was constructed easily at a more reasonable cost, compared to the standard phantom.

► *Please cite this article as:*
Asiah RH, Sutanto H, Anam C, Arifin Z, Bahrudin B, Hilmawati R. Development of In-House Head Computed Tomography Dose Index Phantoms Based On Polyester-Resin Materials. Iran J Med Phys 2021; 18: 255-262. 10.22038/ijmp.2020.46387.1728.

Introduction

Computed tomography (CT), as a complex imaging modality, produces excellent image quality within a short acquisition time at low cost [1–3]. CT scan is widely used for many clinical purposes [4–8]. However, the radiation dose of CT is relatively higher than that of other imaging modalities and may expose patients to a high risk of complications. Accordingly, regular CT dose monitoring is of great significance in medical practice [4, 9, 10]. In other words, CT dose measurement, as an integral part of quality control (QC) programs, must be carried out periodically [11].

The radiation output of CT is obtained from the CT dosimetry and is specifically called the CT dose index (CTDI) [12, 13]. The CTDI, as a dose index, is useful for dose comparisons, dose monitoring, and dose optimization, while it does not represent the patient dose [14–16]. This index has several derivatives, including $CTDI_{air}$, $CTDI_{100}$, $CTDI_{100,c}$, $CTDI_{100,p}$, $CTDI_w$, and $CTDI_{vol}$ [17]. Generally, for CTDI measurements, a standard phantom with a cylindrical shape (head and body phantom diameters, 16 cm and 32 cm, respectively), made of polymethyl methacrylate (PMMA) materials, is used [14, 18–20]. There are five holes inside these phantoms, used to insert a radiation detector and measure doses at different sites.

The $CTDI_{100}$ shows that the dose is measured using a detector with an active length of 100 mm. $CTDI_{100,c}$ and $CTDI_{100,p}$ represent measurements of $CTDI_{100}$ in the central and peripheral holes of the reference phantom. Also, $CTDI_w$ represents a weighted dose measured from five holes, and $CTDI_{vol}$ represents the average dose in the entire phantom volume in a series of scans [5, 6, 9, 11, 18]. Evidence shows that the CTDI is strongly influenced by several input factors, including the tube voltage (kVp) and tube loading (mAs) [21].

The CTDI measurements are carried out, using a pencil ionization chamber, a CT dose profiler, a thermoluminescence detector (TLD), or other types of detectors [22–24]. In the $CTDI_w$ measurements, the availability of CTDI phantom is essential [17]. On the other hand, the $CTDI_{air}$ measurements are conducted in air; therefore, the CTDI phantom is not required [18]. The availability of standard polymethyl methacrylate (PMMA) phantoms for $CTDI_w$ measurements may not be an issue in developed

*Corresponding Author: Tel: +62 (24) 74680822; Fax: +62 (24) 74680822; Email: anam@fisika.fsm.undip.ac.id

countries. However, in some developing countries, such as Indonesia, it poses significant challenges, as PMMA phantoms may not be available due to their high cost. Almost half of CT centers in Indonesia do not have access to standard PMMA phantoms. Therefore, development of alternative phantoms with comparable dose results, using materials that are less expensive, easy to produce, and available in the market, would be very helpful. Also, development of alternative phantoms can help hospitals without access to standard PMMA phantoms to develop suitable physical phantoms for QC programs.

An alternative phantom should have physical parameters, resembling the standard PMMA phantom. The physical parameters primarily include the material density and the effective atomic number (Z_{eff}) [25, 26]. The PMMA density and Z_{eff} are 1.19 g/cm^3 and 6.5, respectively [27]. Materials, such as high-density polyethylene (HDPE), polystyrene, solid water, and acrylonitrile butadiene styrene (ABS), have densities of 0.95, 1.06, 1.04, and 1.04 g/cm^3, respectively [1, 2, 28–30]; therefore, they may be used in the development of alternative CTDI phantoms.

Resin materials are frequently used in daily life. These materials, with a density of 1.00 g/cm^3, may be suitable for alternative CTDI phantoms. In previous study, they were used for simulating the human liver [31]. Besides non-toxicity, resin has high availability and scratch resistance [32]. There are generally two types of resins, that is, epoxy and polyester. The color of epoxy resin is clear yellow, whereas the polyester-resin (PESR) is clear white. Also, PESR is easier to handle than the epoxy resin. Therefore, development of a CTDI phantom from PESR material will be useful. In our preliminary study on development of the CTDI phantoms based on PESR material [33], we investigated their CT number and compared them to those from standard PMMA phantom. We found that CT numbers of the PESR phantoms are 1-9% higher than those of PMMA phantom. Therefore, comprehensive study on CTDI values have not been carried out. Therefore, in this study, we aimed to develop a head CTDI phantom from PESR as an alternative to the standard PMMA phantom and investigate their CTDI values. The CTDI values of developed alternative phantom was compared with the standard PMMA phantom.

Materials and Methods

2.1. Fabrication of alternative CTDI phantoms

The head CTDI phantoms were made from PESR (Yukalac 157 BQTN-EX, PT Justus Kimiaraya, Indonesia) and its catalyst. The chemical formula of PESR is OCO–CH_2–CH_2–COO–CH–CH–O. PESR is a type of unsaturated polyester, with viscosity of 250-350 cP at 250°C, density of 1.09 g.cm^{-3}, modulus elasticity of 3.3 GPa, and heat distortion temperature of 85°C [34]. MEKP (Mepoxe M, PT Justus Kimiaraya, Indonesia) was used as the catalyst in this study. The ratio of MEKP to PESR varied from 1:150 to 1:300. The PESR and the catalyst were manually mixed by stirring for two minutes, and high temperatures, which cause the phantom to break down after drying, were avoided. Afterward, the mixture was poured into a mold for several hours until it hardened at room temperature. The mold used in this study consisted of polyvinyl chloride (PVC) pipes (PT Wahana Duta Jaya Rucika, Jakarta, Indonesia), available in the market. The diameter and height of the pipe were 16 cm and 17 cm, respectively, as shown in Figure 1. Also, the holes in the phantoms were made through a drilling process.

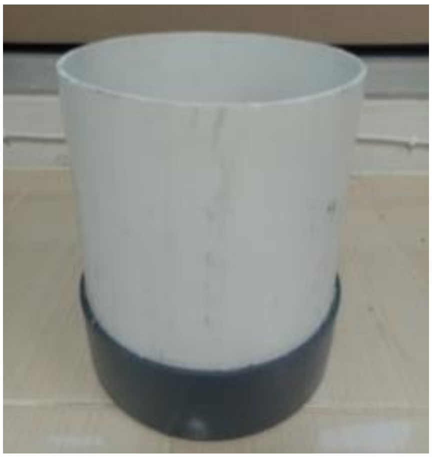

Figure 1. A PVC polymer used for molding the head phantom

Phantom characteristics

The head density of the PESR-MEKP phantom was measured by dividing the mass of the developed PESR-MEKP phantom by its volume [35]. The mass of the PESR-MEKP phantom was measured using a digital scale, while its volume was calculated, based on the dimensions of the phantom. The electron density (number of electrons per gram) was calculated using the following equation [36, 37]:

$$\rho_e = N_A \times \sum \frac{f_i Z_i}{A_i} \quad (1)$$

where N_A is the Avogadro's number (6.022×10^{23}), and f_i, Z_i, and A_i are the weight fraction, the atomic number, and the atomic mass of each atom, respectively.

Moreover, the effective atomic number (Z_{eff}) was calculated using the following equation [38]:

$$Z_{eff} = \sqrt[2.94]{\sum_i f_i \times (Z_i)^{2.94}} \quad (2)$$

The phantom homogeneity was determined by conducting CT scans on the regions of interest (ROIs) at 3, 6, 9, and 12 o'clock positions and at the center of the phantom with the same diameter (Figure 2). The homogeneity was calculated using the following equation [39]:

$$H = \left(1 - \frac{|CT-number_{max} - CT-number_{min}|}{CT-number_{min}} \times 100\%\right) \quad (3)$$

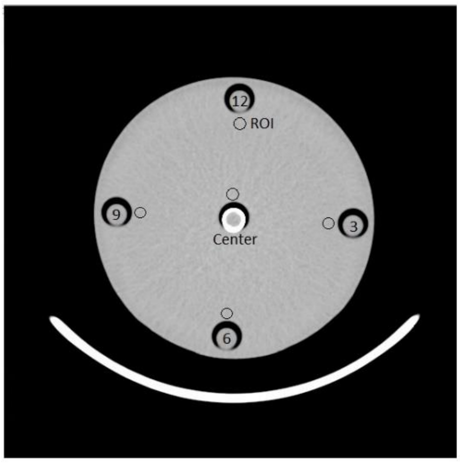

Figure 2. The ROIs for CT number measurements. One ROI and four ROI holes can be found at the peripheries of the phantom

$CTDI_{100}$ measurements

The $CTDI_{100}$ measurements were performed on all holes of the PESR-MEKP phantom and the standard PMMA phantom (CIRS, USA) [24, 40, 41]. The measurements were carried out, using a Philips Brilliance 16-slice CT scanner, a CT dose profiler (RTI Electronics, Sweden), and a Black Piranha electrometer (RTI Electronics, Sweden). The CT dose profiler was a solid-state detector, specifically designed for CTDI measurements in a standard PMMA phantom. The CT dose profiler was connected to the fast Black Piranha electrometer, with a dose rate of 67 nGy/s to 2.2 Gy/s, spatial resolution of 0.25 mm, and inaccuracy of ±5% [42]. The CT dose profiler used the helical mode for measuring the CTDI. It was a small detector, capturing the point dose in real time. By using the helical scan, a dose profile along the Z-axis can be obtained. By integrating this dose profile, the integral dose can be obtained, as it is measured by a pencil chamber in the axial mode [43].

For the scanning process, the phantom was placed on a table, and the center of the phantom was set at the isocenter (Figure 3). The phantom position was expected to remain unchanged during the scanning process. Next, topography was performed to determine the phantom position and the scanning length required. The scanning protocol included the head CT scan protocol with parameters shown in Table 1. Afterward, the CT dose profiler was inserted into a hole of the phantom, and the other holes were closed with acrylic rods. Then, the CT dose profiler was connected to the Black Piranha electrometer, and the electrometer was connected to a laptop to observe the results using the Ocean software [44].

$CTDI_w$ and $CTDI_{vol}$ calculations

The weighted CTDI ($CTDI_w$) was calculated by determining the weighted $CTDI_{100}$ from five holes in the phantoms (Figure 3). The weighting process was carried out based on Equation (4):

$$CTDI_w = \frac{1}{3}CTDI_{100,c} + \frac{2}{3}CTDI_{100,p.} \quad (4)$$

where $CTDI_{100,c}$ is the CTDI value measured in the center of the phantom; and $CTDI_{100,p}$ is the average of doses measured at the periphery of the phantom. By dividing $CTDI_w$ by pitch, the volumetric CTDI ($CTDI_{vol}$) can be obtained. Also, pitch is a table shift divided by the total collimation [5, 9]. However, due to measurements in the helical mode, the pitch was automatically included in the obtained dose profiles.

Percentage differences

After obtaining the $CTDI_w$ and $CTDI_{vol}$ values, the percentage differences between the developed PESR-MEKP phantoms and the standard PMMA phantom were determined, based on the following equation:

$$\%Difference = \frac{A-B}{A} \times 100\%. \quad (5)$$

where *A* denotes the CTDI measured in the standard PMMA phantom, and *B* denotes the CTDI measured in the PESR-MEKP phantom [45].

P-value measurements

To determine whether the developed PESR-MEKP phantom and the standard PMMA phantom are significantly different or not, a statistical test is needed. A t-test was used for this purpose, and P-value less than 0.05 was considered statistically significant [46]. The statistical test was performed with Matlab R14 software (Mathworks Inc., Natick, MA, USA).

Figure 3. The $CTDI_{100}$ measurement using the PESR-MEKP phantom

Table 1. Scan parameters of the head CTDI phantoms

Scan parameter	Setting
Tube voltage (kVp)	120
Tube current-rotation time (mAs)	200
Mode	Helical
Pitch	1
Slice thickness (mm)	5
Total time (s)	11.463

Results

Fabrication of PESR-MEKP phantom

The alternative head CTDI phantoms, based on the PESR-MEKP material, were successfully developed, as shown in Figure 4. The phantoms were in a cylindrical shape and contained five holes with diameters of 1.31 cm for dose measurements. The length and diameter of each phantom were 15 cm and 16 cm, respectively. The ratios of the catalyst (MEKP) to PESR were 1:150, 1:200, 1:250, and 1:300, respectively. Visually, all phantoms were transparent.

Density, electron density, and effective atomic number of the phantom

After mass and volume measurements of the phantom, the density of the PESR-MEKP phantom was calculated. The masses were 3.268, 3.276, 3.214, and 3.218 g for MEKP-to-PESR ratios of 1:150, 1:200, 1:250, and 1:300, respectively. The masses of the head PESR-MEKP phantoms were almost the same, while the volume was 2.829 cm^3. The overall density of the developed phantoms can be seen in Table 2. Also, the density of the standard head CTDI phantom, made of PMMA, was 1.19 g/cm^3 [23]. Therefore, there are only slight differences in density between the standard PMMA phantom and the developed PESR-MEKP phantoms.

The electron density and effective nuclear charge (Z_{eff}) of PESR were 3.48×10^{23} electrons per gram and 7.2, respectively, whereas the electron density and Z_{eff} of PMMA were 3.45×10^{23} electrons per gram and 6.5, respectively. Therefore, the electron density and Z_{eff} of PESR were comparable to the PMMA material.

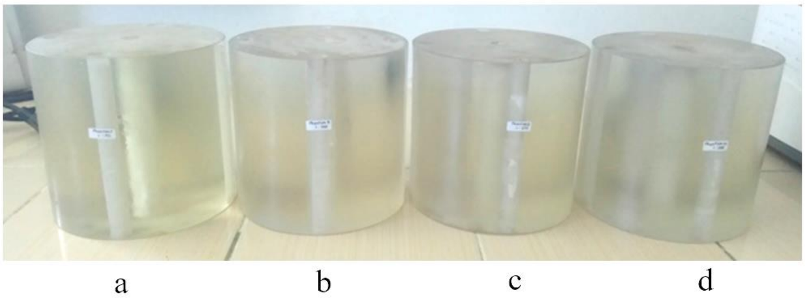

Figure 4. The developed PESR-MEKP phantoms with various MEKP-to-PESR ratios: (a) 1:150, (b) 1:200, (c) 1:250, and (d) 1:300

Table 2. The densities of PESR-MEKP phantoms at various MEKP-to-PESR ratios and their percentage differences with the standard PMMA phantom

MEKP-to-PESR ratio	Density (g/cm^3)	Percentage difference with the PMMA phantom (%)
1:150	1.16 ± 0.01	2.93
1:200	1.16 ± 0.01	2.69
1:250	1.14 ± 0.01	4.53
1:300	1.14 ± 0.00	4.41

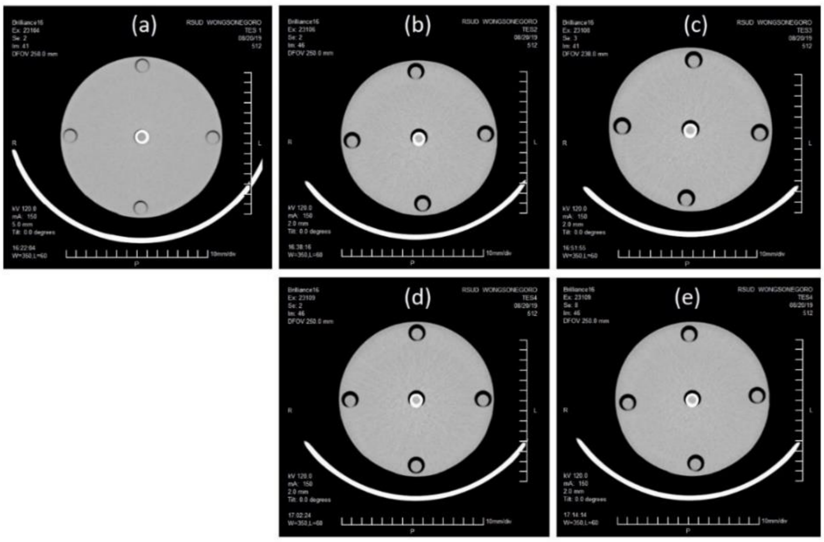

Figure 5. Images of phantoms: (a) Standard PMMA phantom; (b) PESR-MEKP phantom with a ratio of 1:150; (c) PESR-MEKP phantom with a ratio of 1:200; (d) PESR-MEKP phantom with a ratio of 1:250; and (e) PESR-MEKP phantom with a ratio of 1:300

Phantom images and homogeneity

The images of the standard PMMA phantom and the PESR-MEKP phantoms, with MEKP-to-PESR ratios of 1:150, 1:200, 1:250, and 1:300, are shown in Figure 5. It seems that all images of the PESR-MEKP phantom were similar to the standard PMMA phantom. The homogeneity of the developed PESR-MEKP phantoms, with MEKP-to-PESR ratios of 1:150, 1:200, 1:250, and 1:300, is presented in Table 3. The homogeneity of the standard PMMA phantom reached 83.82%, which exceeded all PESR-MEKP phantoms. In the PESR-MEKP phantoms, the lowest homogeneity was found at a ratio of 1:200, with a percentage difference of 9.00% with the standard PMMA phantom, while the greatest homogeneity was observed at a ratio of 1:300 (4.71%).

$CTDI_{100}$, $CTDI_w$, and $CTDI_{vol}$

The $CTDI_{100}$ values for each hole of the phantoms are presented in Table 4. It was found that the $CTDI_{100}$ and $CTDI_w$ values in the developed PESR-MEKP phantoms were slightly higher than those of the standard PMMA phantom, because the resin density was slightly smaller than the standard PMMA phantom (Table 2); therefore, less X-ray attenuation was observed [31]. The percentage differences in $CTDI_{100}$ values between the PESR-MEKP phantoms with ratios of 1:150, 1:200, 1:250, and 1:300 and the standard PMMA phantom are shown in Figure 6. The average differences in CTDI values between the standard PMMA phantom and the alternative PESR-MEKP phantoms with ratios of 1:150, 1:200, 1:250, and 1:300 were 8.5%, 7.0%, 8.8%, and 7.0%, respectively. P-value above 0.05 was only found in the PESR-MEKP phantom with a ratio of 1:300. In other words, the phantom with this ratio showed the greatest resemblance to the standard PMMA phantom.

Table 3. The homogeneities of PESR-MEKP phantoms at various MEKP-to-PESR ratios and their percentage differences with the standard PMMA phantom

MEKP-PESR Ratio	Homogeneity (%)	Percentage difference with the PMMA phantom (%)
1:150	78.6 ± 0.5	6.2 ± 0.2
1:200	76.3 ± 1.5	9.0 ± 0.2
1:250	79.4 ± 1.0	5.3 ± 0.4
1:300	79.9 ± 1.3	4.7 ± 0.3

Table 4. The CTDI values of PMMA and the developed PESR-MEKP phantoms

Parameters	Dose (mGy)				
	Standard	1:150	1:200	1:250	1:300
$CTDI_{100,c}$	26.14 ± 0.01	27.74 ± 0.13	26.97 ± 0.06	27.95 ± 0.02	26.60 ± 0.14
$CTDI_{100,p}$ at 3 o'clock	23.64 ± 0.46	27.24 ± 0.65	27.66 ± 1.43	27.28 ± 0.14	27.29 ± 1.36
$CTDI_{100,p}$ at 6 o'clock	24.95 ± 0.96	28.33 ± 2.40	26.54 ± 1.97	28.29 ± 0.45	28.47 ± 1.70
$CTDI_{100,p}$ at 9 o'clock	27.74 ± 1.37	27.96 ± 1.02	28.09 ± 1.01	27.97 ± 1.34	27.84 ± 1.31
$CTDI_{100,p}$ at 12 o'clock	25.29 ± 1.93	27.02 ± 1.79	27.16 ± 1.23	27.24 ± 0.64	24.39 ± 1.91
$CTDI_w$	25.65 ± 0.79	27.67 ± 1.02	27.23 ± 0.96	27.78 ± 0.44	26.87 ± 1.09
P-value	-	0.045	0.015	0.015	0.200

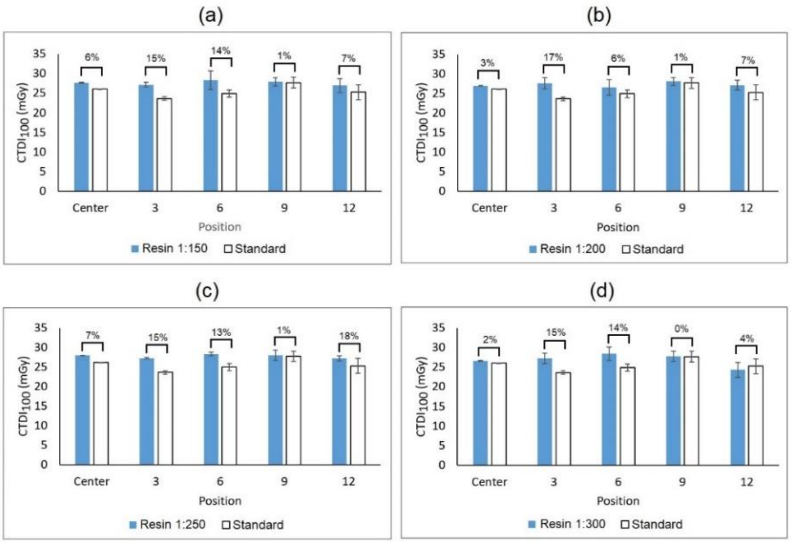

Figure 6. Percentage differences of $CTDI_{100}$ values between the PMMA phantom and the developed PESR-MEKP phantoms at MEKP-to-PESR ratios of: (a) 1:150, (b) 1:200, (c) 1:250, and (d) 1:300 (detector inaccuracy, ±5%)

The $CTDI_w$ values for each phantom are shown in Figure 7. The $CTDI_{vol}$ values were equal to the $CTDI_w$ values, as the pitch value is one. The $CTDI_w$ values of the developed PESR-MEKP phantoms were slightly higher than that of the standard PMMA phantom, with percentage differences of 8%, 6%, 8%, and 5% for ratios of 1:150, 1:200, 1:250, and 1:300, respectively. The EKP-to-PESR ratio of 1:300 showed the smallest percentage difference with the standard PMMA phantom.

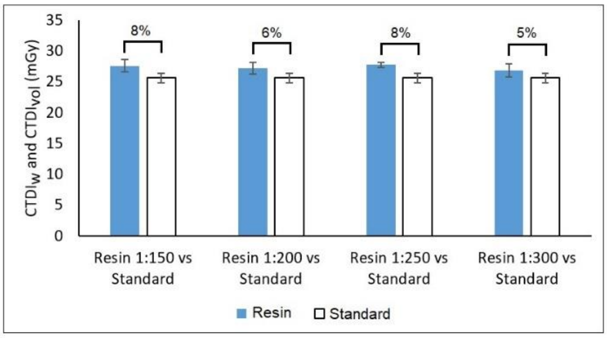

Figure 7. The $CTDI_w$ values for the standard PMMA phantom and the developed PESR-MEKP phantoms

Discussion

The CTDI phantom is essential for CT dose measurements. However, the standard PMMA phantom may not be available in some CT centers in developing countries, as it is not cost-effective. Therefore, the development of alternative phantoms using cheaper materials can help hospitals monitor the CTDI of CT machines. In this study, alternative CTDI phantoms were designed from the PESR material and MEKP as a catalyst. The PESR material was selected, because its density and effective atomic number are relatively close to the standard PMMA phantom; it is also cost-effective and available in the market.

The density of the alternative PESR-MEKP phantoms ranged from 1.14 to 1.16 g/cm^3. Overall, the use of catalysts affects the phantom density. According to the results of the present study, the higher amount of MEKP as the catalyst leads to the greater density of the phantom. The density of the alternative phantom with a MEKP-to-PESR ratio of 1:200 showed the greatest resemblance to the standard PMMA phantom, with a percentage difference of 2.69%. The percentage differences of $CTDI_{100}$ values between the PESR-MEKP phantoms and the standard PMMA phantom were measured in each phantom hole. The dose differences between the PESR-MEKP and PMMA phantoms were influenced by the phantom density and uncertainty of measurements. Based on the current results, the $CTDI_{100,p}$ value at the 9 o'clock position had the smallest percentage difference with the standard phantom, compared to the other holes. In contrast, the $CTDI_{100,p}$ value at the 6 o'clock position had the greatest percentage difference with the standard phantom, compared to the other holes; however, these differences were very small and within the measurement uncertainty range.

The percentage differences of $CTDI_w$ values between the standard phantom and the PESR-MEKP phantoms with ratios of 1:150, 1:200, 1:250, and 1:300 were 8%, 6%, 8%, and 5%, respectively (Figure 7). The smallest percentage difference was obtained at a ratio of 1:300. Overall, the percentage differences were still considered acceptable, because the allowed percentage difference is ±20% [42]. Moreover, statistical t-test was carried out to determine significant differences. The P-value for the PESR-MEKP phantom with a ratio of 1:300 was above 0.05, indicating no significant difference with the standard PMMA phantom.

In the process of phantom development, PESR was mixed with the catalyst as a hardener. For one phantom, the total required mass of PESR and catalyst was about 3 kg, and PESR was widely available in the market at a price around $4 per kilogram; therefore, its cost is very low. Moreover, the development process is fairly simple, because it does not require any special tools, and the process is straightforward. Since our phantom is far cheaper than the standard PMMA phantom and has a simple and rapid manufacturing process, its development seems reasonable. However, it should be noted that this phantom is an in-house phantom, and repeatability is not guaranteed. Therefore, it is only suitable as an alternative when a standard phantom does not exist.

Efforts have been made to develop in-house CTDI phantoms. In this regard, Akpochafor et al. [47] developed a CTDI phantom from PMMA, which could be filled with water. The phantom was validated with a standard phantom. Their results showed no significant difference in the average dose between the developed and standard phantoms (P=0.06). Also, the percentage difference of dose between the developed and standard phantoms was 19.8% [47]. However, the results of the current study are more acceptable than the mentioned study.

In another study, Saravanakumar et al. [23] developed in-house pediatric head and body CTDI phantoms, using PMMA materials. The percentage differences of $CTDI_{vol}$ between the artificial PMMA phantoms and the standard phantom were 16.62%, 10.32%, 2.68%, and 1.42% for voltage variations of 70, 80, 100, and 120 kVp, respectively [23]. Although this study reported better results for a tube voltage of 120 kVp, compared to the current study, it should be noted that the phantom was composed of PMMA materials. In other words, the materials used in their phantoms and the standard phantom were the same.

In the present study, the developed phantom was only a head phantom. However, a 1:300 composition is still applicable to other sizes of the phantom. In future studies, phantoms with a diameter of 32 cm can be developed for body measurements [23, 45]. Also, phantoms with various diameters for measuring the size-specific dose estimates need to be developed [48]. Moreover, it is necessary to develop phantoms with length variations for evaluating the equilibrium doses, as well as phantoms with different shapes for assessing the tube current modulation [16].

Conclusion

The alternative head phantoms from the PESR-MEKP material were successfully developed with varying ratios of 1:150 to 1:300. The PESR-MEKP phantom with a ratio of 1:300 showed an insignificant difference with the standard PMMA phantom. The difference with the standard PMMA phantom in terms of the $CTDI_w$ values was only 5%. Based on the present results, the PESR-MEKP phantom is cost-effective and easy to develop. Therefore, it may be useful for CT centers without access to standard PMMA phantoms for dose measurements.

Acknowledgment

This study was funded by the World Class Research University (WCRU), Diponegoro University, Contract number: 118-11/UN7.6.1/PP/2021.

References

1. Roa AM, Andersen HK, Martinsen AC. CT image quality over time: comparison of image quality for six different CT scanners over a six-year period. Journal of applied clinical medical physics. 2015 Mar;16(2):350-65.
2. Jones AK, Hintenlang DE, Bolch WE. Tissue-equivalent materials for construction of tomographic dosimetry phantoms in pediatric radiology. Medical physics. 2003 Aug;30(8):2072-81.
3. Tack D, Kalra MK, Gevenois PA, editors. Radiation dose from multidetector CT. Springer Science & Business Media; 2012 Jun 5.
4. Brenner DJ, Hall EJ. Computed tomography−an increasing source of radiation exposure. New England Journal of Medicine. 2007 Nov 29;357(22):2277-84.
5. Bushberg JT, Seibert JA, Leidholdt EM Jr, Boone JM. The Essential Physics of Medical Imaging, 3rd ed. Philadelphia: Lippincott William & Wilkins, a Wolters Kluwer Business. 2012.
6. Seeram E. Computed Tomography: Physical Principles, Clinical Application, and Quality Control, 4th ed. Australia: Elsevier. 2009.
7. Moloney F, Twomey M, James K, Kavanagh RG, Fama D, O'Neill S, et al. A phantom study of the performance of model-based iterative reconstruction in low-dose chest and abdominal CT: When are benefits maximized?. Radiography. 2018 Nov 1;24(4):345-51. DOI: 10.1016/j.radi.2018.04.010.
8. Mansour Z, Mokhtar A, Sarhan A, Ahmed MT, El-Diasty T. Quality control of CT image using American College of Radiology (ACR) phantom. The Egyptian Journal of Radiology and Nuclear Medicine. 2016 Dec 1;47(4):1665-71. DOI: 10.1016/j.ejrnm.2016.08.016.
9. Haba T, Koyama S. Estimation of suitable CTDI phantom diameter for standard Japanese body size. European Congress of Radiology-ECR 2013. DOI: 10.1594/ecr2013/C-1782.
10. Bauhs JA, Vrieze TJ, Primak AN, Bruesewitz MR, McCollough CH. CT dosimetry: comparison of measurement techniques and devices. Radiographics. 2008 Jan;28(1):245-53. DOI: 10.1148/rg.281075024.
11. McCollough C, Cody D, Edyvean S, Geise R, Gould B, Keat N, et al. The measurement, reporting, and management of radiation dose in CT. Report of AAPM Task Group. 2008 Jan;23(23):1-28.
12. Shope TB, Gagne RM, Johnson GC. A method for describing the doses delivered by transmission x-ray computed tomography. Medical physics. 1981 Jul;8(4):488-95. DOI: 10.1118/1.594995.
13. McCollough CH, Leng S, Yu L, Cody DD, Boone JM, McNitt-Gray MF. CT dose index and patient dose: they are not the same thing. Radiology. 2011 May;259(2):311-6.
14. Choi HR, Kim RE, Heo CW, Kim CW, Yoo MS, Lee Y. Optimization of dose and image quality using self-produced phantom with various diameters in pediatric abdominal CT scan. Optik. 2018 Sep 1;168:54-60. DOI: 10.1016/j.ijleo.2018.04.066.
15. Anam C, Haryanto F, Widita R, Arif I, Dougherty G. A fully automated calculation of size-specific dose estimates (SSDE) in thoracic and head CT examinations. Journal of Physics: Conference Series 2016 Mar 1;694(1):012030. IOP Publishing. DOI: 10.1088/1742-6596/694/1/012030.
16. Anam C, Haryanto F, Widita R, Arif I, Dougherty G, McLean D. Volume computed tomography dose index (CTDIvol) and size-specific dose estimate (SSDE) for tube current modulation (TCM) in CT scanning. International Journal of Radiation Research. 2018 Jul 1;16(3):289-97. DOI: 10.18869/acadpub.ijrr.16.2.289.
17. McNitt-Gray MF. AAPM/RSNA physics tutorial for residents: topics in CT: radiation dose in CT. Radiographics. 2002 Nov;22(6):1541-53. DOI: 10.1148/rg.226025128.
18. Bujila R, Kull L, Danielsson M, Andersson J. Applying three different methods of measuring CTDIfree air to the extended CTDI formalism for wide‐beam scanners (IEC 60601‐2‐44): A comparative study. Journal of applied clinical medical physics. 2018 Jul;19(4):281-9. DOI: 10.1002/acm2.12363.
19. Boone JM. The trouble with CTDI100, 2007 Med. Phys.;34(4):1364-71. DOI: 10.1118/1.2713240.
20. Tsapaki V, Rehani M. Dose management in CT facility. Biomedical imaging and intervention journal. 2007 Apr;3(2). DOI: 10.2349/biij.3.2.e43.
21. Din NN, Zainon R, Rahman AT. Evaluation of radiation dose in pediatric head CT examination: a phantom study. InIOP Conference Series: Materials Science and Engineering. 2018; 298(1):012046. IOP Publishing. DOI: 10.1088/1757-899X/298/1/012046.
22. Descamps C, Gonzalez M, Garrigo E, Germanier A, Venencia C. SU-E-T-532: Measurements of the Doses Delivered during Radiotherapy CT Exams Using AAPM Task Group Report No 111. Medical physics. 2011 Jun;38(6Part19):3611. DOI: 10.1118/1.3612494.
23. Saravanakumar A, Vaideki K, Govindarajan KN, Jayakumar S, Devanand B. Cost-effective pediatric head and body phantoms for computed tomography dosimetry and its evaluation using pencil ion chamber and CT dose profiler. Journal of Medical

Physics/Association of Medical Physicists of India. 2015 Jul;40(3):170. DOI: 10.4103/0971-6203.165073.
24. Anam C, Haryanto F, Widita R, Arif I, Fujibuchi T, Toyoda T, Dougherty G. Scatter index measurement using a CT dose profiler. J Med Phys Biop. 2017 Sep 4;4:95-102.
25. Yohannes I, Kolditz D, Langner O, Kalender WA. A formulation of tissue-and water-equivalent materials using the stoichiometric analysis method for CT-number calibration in radiotherapy treatment planning. Physics in Medicine & Biology. 2012 Feb 14;57(5):1173. DOI: 10.1088/0031-9155/57/5/1173.
26. Marashdeh MW, Alshipli M, Kabir NA, Tajuddin AA, Hashim R. Evaluating the Physical Properties of Epoxy Resin as a Phantom Material to Mimic the Human Liver in Computed Tomography Applications. IJACEBS. 2018;5(1):22‑6.
27. Johns HE, Cunningham JR. The physics of radiology. 4th ed. Charles C Thomas Publisher. 1983.
28. Groenewald A, Groenewald WA. Development of a universal medical X-ray imaging phantom prototype. Journal of applied clinical medical physics. 2016 Nov;17(6):356-65.
29. Kumar R, Sharma SD, Despande S, Ghadi Y, Shaiju VS, Amols HI, et al. Acrylonitrile Butadiene Styrene (ABS) plastic-based low cost tissue equivalent phantom for verification dosimetry in IMRT. Journal of Applied Clinical Medical Physics. 2010 Dec;11(1):24-32.
30. Groenewald A, Groenewald WA. In-house development of a neonatal chest simulation phantom. Journal of applied clinical medical physics. 2014 May;15(3):282-96. DOI: 10.1120/jacmp.v15i3.4768.
31. Meredith WJ, Massey JB. Fundamental physics of radiology. Butterworth-Heinemann; 2013 Oct 22.
32. Strzelec K. Studies on the properties of epoxy resins cured with polythiourethanes. International journal of adhesion and adhesives. 2007 Mar 1;27(2):92-101. DOI: 10.1016/j.ijadhadh.2006.02.001.
33. Hilmawati R, Sutanto H, Anam C, Arifin Z, Asiah RH, Soedarsono JH. Development of a head CT dose index (CTDI) phantom based on polyester resin and methyl ethyl ketone peroxide (MEKP): a preliminary study. Journal of Radiological Protection. 2020 Jun;40(2):544-553. DOI: 10.1088/1361-6498/ab81a6.
34. Reis JM, Jurumenh MA. Experimental investigation on the effects of recycled aggregate on fracture behavior of polymer concrete. Materials Research. 2011 Sep;14(3):326-30. DOI: 10.1590/S1516-14392011005000060.
35. Halliday D, Resnick R, Walker J. Fundamentals of physics. John Wiley & Sons; 2013 Aug 13.
36. Chang KP, Hung SH, Chie YH, Shiau AC, Huang RJ. A comparison of physical and dosimetric properties of lung substitute materials. Medical physics. 2012 Apr;39(4):2013-20. DOI: 10.1118/1.3694097.
37. Amini I, Akhlaghi P, Sarbakhsh P. Construction and verification of a physical chest phantom from suitable tissue equivalent materials for computed tomography examinations. Radiation Physics and Chemistry. 2018 Sep 1;150:51-7. DOI: 10.1016/j.radphyschem.2018.04.020.
38. Qi Z, Zambelli J, Bevins N, Chen GH. Quantitative imaging of electron density and effective atomic number using phase contrast CT. Physics in Medicine & Biology. 2010 Apr 19;55(9):2669. DOI: 10.1088/0031-9155/55/9/016.
39. Irdawati Y, Sutanto H, Anam C, Fujibuchi T, Zahroh F, Dougherty G. Development of a novel artifact-free eye shield based on silicon rubber-lead composition in the CT examination of the head. Journal of Radiological Protection. 2019 Sep 24;39(4):991. DOI: 10.1088/1361-6498/ab2f3e.
40. Goldman LW. Principles of CT: multislice CT. Journal of nuclear medicine technology. 2008 Jun 1;36(2):57-68. DOI: 10.2967/jnmt.107.044826.
41. Toth TL. Dose reduction opportunities for CT scanners. Pediatric radiology. 2002 Apr 1;32(4):261. DOI: 10.1007/s00247-002-0678-7.
42. RTI Electronic. CT Dose Summary. RTI Electronic. 2009.
43. Corona EC, Ferreira IB, Herrera JG, López S, Covarrubias O. Verification of CTDI and DLP values for a head tomography reported by the manufacturers of the CT scanners, using a CT dose profiler probe, a head phantom and a piranha electrometer. ISSSD (2015). 2015:426-35.
44. Anam C, Fujibuchi T, Haryanto F, Widita R, Arif I, Dougherty G. An evaluation of computed tomography dose index measurements using a pencil ionisation chamber and small detectors. Journal of Radiological Protection. 2019 Jan 4;39(1):112. DOI: 10.1088/1361-6498/aaf2b4.
45. Cannillo B, Ostan A, Dionisi C, Fusco G, Carriero A, Brambilla M. Variability of the discrepancy between manufacturer and measured CTDI100 values by scanner type, acquisition parameters and phantom size. Physica Medica. 2018 May 1;49:34-9. DOI: 10.1016/j.ejmp.2018.04.390.
46. Vital KD, Mendes BM, de Sousa Lacerda MA, da Silva TA, Fonseca TC. Development of a physical head phantom using of a solid brain equivalent tissue for the calibration of the 18F-FDG internal monitoring system. Radiation Physics and Chemistry. 2019 Feb 1;155:56-61. DOI: 10.1016/j.radphyschem.2018.08.037.
47. Akpochafor MO, Adeneye SO, Ololade K, Omojola AD, Adedewe N, Adedokun A, et al. Development of computed tomography head and body phantom for organ dosimetry. Iranian Journal of Medical Physics. 2019;16(1):8-14. DOI: 10.22038/ijmp.2018.30906.1360.
48. Anam C, Haryanto F, Widita R, Arif I, Dougherty G. Automated calculation of water-equivalent diameter (DW) based on AAPM task group 220. Journal of applied clinical medical physics. 2016 Jul;17(4):320-33. DOI: 10.1120/jacmp.v17i4.6171.